Received 15 November 2021; revised 13 December 2021; accepted 16 December 2021. Date of publication 21 December 2021; date of current version 5 January 2022.

Digital Object Identifier 10.1109/OJAP.2021.3136903

Unified Reciprocal Space Processing for Short-Range Active and Passive Imaging Systems

AARON V. DIEBOLD[1], THOMAS FROMENTEZE[2], ETTIEN KPRÉ[3], CYRIL DECROZE[2], MOHAMMADREZA F. IMANI[4] (Member, IEEE), AND DAVID R. SMITH[1] (Senior Member, IEEE)

[1]Center for Metamaterials and Integrated Plasmonics, Department of Electrical and Computer Engineering, Duke University, Durham, NC 27708, USA

[2]XLIM, UMR 7252, University of Limoges, 87000 Limoges, France

[3]MC2 Technologies, 59650 Villeneuve d'Ascq, France

[4]School of Electrical, Computer, and Energy Engineering, Arizona State University, Tempe, AZ 85287, USA

CORRESPONDING AUTHOR: A. V. DIEBOLD (e-mail: aaron.diebold@duke.edu)

This work was supported in part by the Air Force Office of Scientific Research under Grant FA9550-18-1-0187.

ABSTRACT Large scale sensing systems increasingly operate in short-range geometries, providing three-dimensional imaging capabilities that leverage the large number of degrees of freedom of distributed arrays. The two most powerful modes of operation include active, multiple-input multiple-output arrays, in which an image is processed from signals measured using different pairs of transmitting and receiving antennas; and passive, synthetic aperture interferometric radiometer arrays, which can image using ambient, non-cooperative radiation by processing signals measured at different receiving antenna pairs. In this paper, we explore the analogy between these two imaging modes, and outline a generalized framework for analyzing these systems in the array near field. Focusing on the similarities between the formalisms describing the operation of generic active and passive systems, it is proposed, to our knowledge for the first time in the scientific literature, to adapt a Fourier-based imaging technique optimized for short-range active MIMO systems to passive technologies, interrogating the emissivity of a spatially distributed target. The systematic method presented in this paper provides a framework for characterizing and optimizing short range coherent or incoherent systems used in threat detection and non-destructive testing applications.

INDEX TERMS Full matrix imaging, interferometers, MIMO radar, multistatic radar, SAIR, short-range imaging.

I. INTRODUCTION

ACHIEVING fast and accurate imaging performance at wavelength-scale resolution is a widespread concern in a growing number of applications, giving rise to a diversity of architectures within the scientific community. Active systems that utilize coherent illumination can recover an image from scattered field measurements, with optimal performance usually realized by multiple-input multiple-output (MIMO) systems that process a complete collection of transmit-receive signal pairs. Such architectures, though largely proposed and demonstrated in large-scale radar applications, are increasingly utilized for buried threat detection [1], [2], [3], [4] and structural monitoring [5], [6] in short-range configurations [7]. Alternatively, passive systems can form images by exploiting ambient radiation with interferometric array measurements. Such systems are referred to as synthetic aperture interferometric radiometers (SAIR). The radiation in these scenarios can be of a thermal nature according to the gray body radiation principle, or can be generated by non-cooperative sources such as radio transmitters and noise sources [8]. In both cases, interferometric processing enables image estimation of the source or scattering structures through signal correlations over an array. As in the case of active systems, techniques pioneered

in large-scale radio frequency systems have since been distilled into deployable systems for passive imaging of noise sources [9], [10], [11], [12] and imaging with ambient wifi signals [13], [14].

Unfortunately, efficiency and resolution criteria pose conflicting demands in both active and passive systems, as high resolution requires large apertures that lengthen acquisition and reconstruction times. Thinned arrays and aperture synthesis techniques that apply virtual array or effective aperture principles [15], [16], [17], [18] can resolve some of these challenges by leveraging redundancy in the sensing task described by shared plane wave or *k-space* contributions [19]. A variety of successful methods pair this perspective with the efficiency of Fourier domain/fast Fourier transform (FFT) processing to alleviate computational reconstruction times [20], [21], [22], [23]. These strategies have largely developed separately in investigations of active/coherent and passive/incoherent systems, though the different modalities often share common objectives. The coarray framework presented in [24] unifies coherent and incoherent imaging systems by describing them as sum and difference coarrays, respectively. Nevertheless, virtual array principles and the coarray description are rigorous only in the far field [17], [25], and the extension to short-range, three-dimensional imaging has not been adequately explored to the authors' knowledge.

Analogies between active MIMO and passive SAIR systems are thus described for short-range imaging geometries in this paper. These efforts will not only allow a more intuitive understanding, but will allow us to adapt techniques from each domain to optimize their operation in the particularly constraining framework of short-range imaging. The objective of this paper is, moreover, to propose a critical analysis of the limitations associated with the use of the concept of virtual arrays, sometimes referred to as effective arrays or co-arrays [24]. In the general framework of aperture synthesis techniques, this principle is applied to MIMO systems [26], [27] as well as to their interferometric duals [28]. Such an approach achieves image reconstruction through processing of data from a virtual array that can approximately replace the true array in the far field of the array. Nevertheless, the validity of such an approximation deteriorates at short imaging distances. It thus seems interesting in the general context of short-range imaging applications to propose image analysis and reconstruction techniques allowing to free oneself from the tools developed in less constrained far-field applications. Plane wave expansion techniques seem to be a suitable answer to such constraints, offering powerful analysis tools to evaluate the performance of imaging systems, accelerated reconstruction techniques using fast Fourier transforms, and a formalism easily adaptable to MIMO or interferometric architectures.

Section II discusses limitations in applying virtual array principles to short-range imaging systems, and introduces the generic MIMO and SAIR systems used in our studies. A brief development of an active MIMO imaging system is then given below in Section III, while that for a passive SAIR system follows in Section IV. Section V contains a unifying Fourier domain description of these systems as well as a reconstruction algorithm adapted from the MIMO radar domain. Finally, we demonstrate the application of these ideas with numerical studies in Section VI.

II. SHORT-RANGE ARRAY IMAGING

As is done in related works [9], [20], [21], [29], a simple short-range imaging array can be modeled using isotropic antennas that transmit and/or receive an electromagnetic signal. While such idealized antennas cannot be realized in practice, they serve as a good approximation for antennas with wide gain patterns interrogating a spatially limited geometry. Moreover, such antennas are well-suited to a variety of short-range imaging applications in which one wishes to give equal weight to all target locations within a wide field of view through uniform illumination. This can in turn maximize the diversity of spatial information measured by the antenna array to optimize the resolution of the computed images. When this approximation fails to hold, the methods proposed here can be extended to include effects of antenna radiation patterns through additional filter terms [30]. In addition, we will further restrict our analysis to that of a scalar signal, e.g., a single Cartesian component of the electric field, which conforms naturally to the isotropic radiator approximation. While a rigorous study considers all vector components of the electric (and/or magnetic fields), an assumption of isotropically scattering or radiating targets allows us to separate these components and treat each independently. Considering the real-time imaging demands of most target applications employing short-range imaging, such reductions in model complexity offer advantages in terms of acquisition and reconstruction speeds, with minor loss in accuracy. For example, depolarization effects have been seen to have relatively minor impact on image quality in a case of practical interest [31]. For these reasons, several works have experimentally validated such approximations [3], [4], [21], [32], [33].

We first develop a justification for the use of isotropic radiating antenna elements and an associated scalar model, which can be similarly applied to the case of receive-mode antennas by the principle of reciprocity. Considering initially the most general case, the radiation of an antenna i must be determined as a function of its vector current distribution $\mathbf{J}_i(\mathbf{r}_i, k)$, $\mathbf{r}_i$ corresponding to the antenna space. By means of an intermediate vector potential omitted here for the sake of compactness and satisfying the Helmholtz equation, the vector electric field $\mathbf{E}_i(\mathbf{r}, k)$ radiated into the target space $\mathbf{r}$ is determined as follows [34], [35], [36]:

$$\mathbf{E}_i(\mathbf{r}, k) = j\mu_0 kc \int_{\mathbf{r_i}} \mathbf{J}_i(\mathbf{r}_i, k) \left(\bar{\mathbf{I}} + \frac{\nabla\nabla}{k^2}\right)\{G(\mathbf{r}, \mathbf{r}_i, k)\}\, d^3\mathbf{r}_i \tag{1}$$

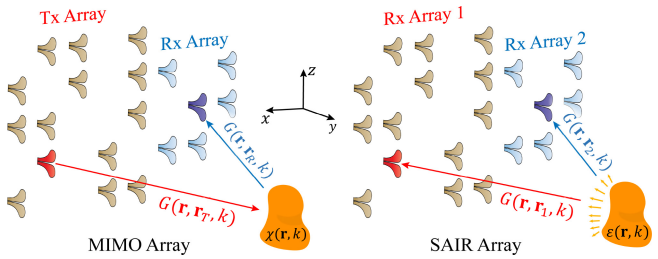

FIGURE 1. Analogy between two generic architectures of MIMO and SAIR systems. Both techniques exploit the combination of the spatial diversities of two antenna arrays. Only the direction of propagation varies on these schemes from the interrogation of the reflection $\chi(\mathbf{r}, k)$ and emission $\varepsilon(\mathbf{r}, k)$ of a target in the region of interest.

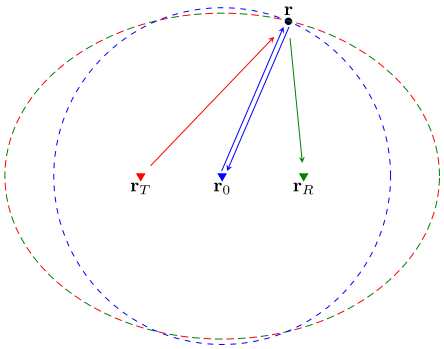

FIGURE 2. Substitution of a transceiver pair interacting with a scene to be imaged by an equivalent mono-static setup. The difference between the domains covered by each approach allows to highlight the limits of such a simplification for aperture synthesis applied to short-range imaging.

where μ_0 corresponds to the magnetic permeability of vacuum, c is the speed of light and $k = 2\pi/\lambda$ is the wavenumber. The term $G(\mathbf{r}, \mathbf{r}_i, k)$ stands for the scalar Green's function, representing the free space propagation between the positions $\mathbf{r}_i$ and $\mathbf{r}$:

$$G(\mathbf{r}_i, \mathbf{r}, k) = \frac{e^{-jk|\mathbf{r}-\mathbf{r}_i|}}{4\pi|\mathbf{r}-\mathbf{r}_i|}. \tag{2}$$

Associated with the operator $(\bar{\mathbf{I}}+\nabla\nabla/k^2)$, one forms a dyadic Green's function that projects the polarization of electric currents into space. By applying a first approximation related to the exploitation of isotropic radiating elements, we consider first that the current distribution can be substituted such as $\mathbf{J}_i(\mathbf{r}_i, k) \rightarrow a\delta(\mathbf{r}_i - \mathbf{r}'_i)$, where a is a normalization constant with units A m, and $\mathbf{r}'_i$ corresponds to the position of the point element. As the latter has by definition no spatial extension, one cannot associate with it a polarization, and it is now necessary to only use a scalar propagation model. By substituting the expression of the current density in the previous equation, we finally obtain the expression for the scalar approximation $E_i(\mathbf{r}, k)$ of the radiated electric field:

$$E_i(\mathbf{r}, k) = j\mu_0 kca \int_{\mathbf{r_i}} \delta\left(\mathbf{r}_i - \mathbf{r}'_i\right)\, G(\mathbf{r}, \mathbf{r}_i, k)\, d^3\mathbf{r}_i \tag{3}$$

$$= j\mu_0 kca G\left(\mathbf{r}, \mathbf{r}'_i, k\right) \tag{4}$$

Under these assumptions, a MIMO radar system consists of isotropic transmitting antennas emitting coherent spherical waves at positions $\mathbf{r}_T$, and isotropic receiving antennas that measure the scattered radiation at wavenumber k and positions $\mathbf{r}_R$ (Fig. 1). An analogous SAIR system for passive imaging employs an array of isotropic receiving antennas at positions $\mathbf{r}_1$, and a second array at positions $\mathbf{r}_2$ that are potentially distinct from those of the first array (Fig. 1). The horizontal and vertical dimensions of these array systems lie in the x and z directions, respectively, while the range or longitudinal direction coincides with the y axis.

The virtual array method consists in substituting the two arrays by a single synthetic aperture capable of interrogating the same information from the scene to be imaged. In the most general and complex context of short-range imaging applications, it consists in finding fictive radiating element positions $\mathbf{r}_0$ guaranteeing $|\mathbf{r}-\mathbf{r}_T|+|\mathbf{r}-\mathbf{r}_R| = 2|\mathbf{r}-\mathbf{r}_0|$ for all combinations of transmitters and receivers (or similarly for $\mathbf{r}_1$ and $\mathbf{r}_2$). A simple geometric interpretation of the problem makes it possible to highlight the limits of such a model (Fig. 2). Considering that the set of loci of $|\mathbf{r}-\mathbf{r}_T|+|\mathbf{r}-\mathbf{r}_R|$ correspond to an ellipsoid whose focal points are occupied by a given pair of transmitter and receiver positions, it does not seem possible to substitute this bi-static arrangement by an equivalent mono-static experiment, represented by a sphere of coordinate $|\mathbf{r}-\mathbf{r}_0|$ centered at $\mathbf{r}_0$.

The imaging techniques proposed in this context generally use first-order Taylor expansions [37], leading to the following expressions:

$$|\mathbf{r}-\mathbf{r}_T| + |\mathbf{r}-\mathbf{r}_R| \approx 2R + \frac{x^2+z^2}{R} + \frac{x_T^2+x_R^2+z_T^2+z_R^2}{2R} - u(x_T+x_R) - v(z_T+z_R) \tag{5}$$

$$|\mathbf{r}-\mathbf{r}_1| - |\mathbf{r}-\mathbf{r}_2| \approx \frac{x_1^2-x_2^2+z_1^2-z_2^2}{2R} + u(x_2-x_1) + v(z_2-z_1) \tag{6}$$

where R corresponds to the longitudinal distance between the antenna arrays, placed in the y = 0 plane, and a plane to be imaged. The direction cosines $u = x/R$ and $v = z/R$ define angles that are directly exploited in far-field approximations. The coordinates multiplied in each case to the director cosines correspond to the positions of the fictive synthetic aperture elements. It is important to keep in mind that these developments are the result of approximations, based on geometrical constraints imposing that the relations $(x-x_T)^2/R^2$, $(x-x_R)^2/R^2$, $(z-z_T)^2/R^2$ and $(z-z_R)^2/R^2$ are all much lower than 1 (and respectively substituting by x_1, z_1, x_2, and z_2 for the interferometric case). If the exploitation of quadratic phase terms identified in equations (5) and (6) makes it possible to partially adapt short-range radiation problems to the concepts of effective arrays initially developed for far field applications [37], it is however necessary to be aware of the limits of such expansions when such approximations do not hold, in particular when reconstructions are carried out far from the stationary phase point used as a reference for these developments.

III. ACTIVE, COHERENT IMAGING

In an active MIMO radar system, the image target can be modeled as a scattering distribution determined by its spatially varying susceptibility $\chi(\mathbf{r}, k)$, which is generally frequency dependent. Upon omitting the magnitude term in Eq. (4) assuming identical antenna current densities, we may express the fields from a given transmitting element at position $\mathbf{r}_T$ as simply $G(\mathbf{r}, \mathbf{r}_T, k)$ and, by reciprocity, from a receiving element at position $\mathbf{r}_R$ as $G(\mathbf{r}, \mathbf{r}_R, k)$. The incident electric fields radiated by a given transmitting antenna excites a polarization current density in the target given by $P(\mathbf{r}) = -j\omega\epsilon_0\chi(\mathbf{r}, k)G(\mathbf{r}, \mathbf{r}_T, k)$. By Poynting's theorem, this current density induces a signal in the receiving antenna according to $\frac{1}{2}P(\mathbf{r})G(\mathbf{r}, \mathbf{r}_R, k)$, so that the interaction of this transmitter-receiver pair with the target results in a signal [21], [36]

$$s(\mathbf{r}_T, \mathbf{r}_R, k) = \int \chi(\mathbf{r}, k)\, G(\mathbf{r}, \mathbf{r}_T, k)\, G(\mathbf{r}, \mathbf{r}_R, k)\, d^3\mathbf{r}, \quad (7)$$

where we have further normalized the signal at each frequency to focus on the propagation terms in the integrand. In addition, the model is simplified by the first Born approximation that considers only single scattering of the incident fields. We find that a MIMO radar system retrieves a set of signals related to the target susceptibility by a pair of Green's function terms.

IV. PASSIVE, INCOHERENT IMAGING

An interferometric array can recover images of noise sources through correlation processing of the signals simultaneously measured at these two receiver arrays. An incoherent source $n(\mathbf{r}, k)$ that radiates or scatters wide-sense stationary, random noise waveforms with uncorrelated frequency components satisfies the second order correlation property [38] $\langle n^*(\mathbf{r}, k)n(\mathbf{r}', k')\rangle = \varepsilon(\mathbf{r}, k)\delta(\mathbf{r}-\mathbf{r}')\delta(k-k')$, where $\varepsilon(\mathbf{r}, k) = \langle n^*(\mathbf{r}, k)n(\mathbf{r}, k)\rangle$ is the spectral density, or the emissivity for radiating bodies, that defines the spatial and frequency content of the image target, and is an observable quantity given suitable averaging over multiple noise realizations, denoted by $\langle\cdot\rangle$. The propagation of this spectral density is governed in short-range geometries by a generalized Van Cittert-Zernike Theorem [39]:

$$v(\mathbf{r}_1, \mathbf{r}_2, k) = \int \varepsilon(\mathbf{r}, k)G^*(\mathbf{r}, \mathbf{r}_1, k)G(\mathbf{r}, \mathbf{r}_2, k)d^3\mathbf{r}, \quad (8)$$

where $G(\mathbf{r}, \mathbf{r}', k)$ is the free space Green's function defined in Eq. (2). The function $v(\mathbf{r}_1, \mathbf{r}_2, k)$ is the aperture-plane visibility function [40], also known as the cross-spectral density [38], measured through cross correlations of noise signals measured at pairs of receiver antennas.

Comparison of equations (7) and (8) reveals a similar structure characterizing the relationship between the target function ($\chi(\mathbf{r}, k)$ or $\varepsilon(\mathbf{r}, k)$) and the array measurements ($s(\mathbf{r}_T, \mathbf{r}_R, k)$ or $v(\mathbf{r}_1, \mathbf{r}_2, k)$) by a pair of propagation terms. In far field operation, this similar structure leads to the well-known, direct Fourier transform relationship between the target function and the synthesized aperture measurements [24]. The only notable difference arises as the conjugation of one of the propagation terms in the passive model. While seemingly minor, this is the fundamental feature of the passive model (Eq. (8)) that leads to its mathematical characterization as an incoherent imaging system, versus the coherent imaging system described by the active model of Eq. (7). Nevertheless, we will show next that we can exploit the similar structure to investigate the point spread function (PSF) characteristics of the two systems through spatial frequency analysis, and ultimately devise a passive Fourier domain imaging algorithm analogous to the range migration algorithm [20], [21], [29] commonly applied in active imagers.

V. K-SPACE REPRESENTATION AND PROCESSING

In long range imaging geometries, array measurements relate to the image target by a Fourier transform [24]—this is true for both active and passive systems. Short-range systems do not possess such a simple relationship. Instead, one can formulate a Fourier domain mapping that describes the three-dimensional properties of the system in terms of three-dimensional spatial frequency, or *k-space*, coverage. Application of this technique to coherent systems is described in [21]. In order to demonstrate the analogy with incoherent systems, we repeat an abbreviated analysis here, before extending the framework to passive SAIR systems.

Our active system data set consists of complex-valued measurements for all pairs of transmitters and receivers in the plane $y = 0$:

$$s(\mathbf{r}_T, \mathbf{r}_R, k) = \int \chi(\mathbf{r}, k)\frac{e^{-jk|\mathbf{r}-\mathbf{r}_T|}}{|\mathbf{r}-\mathbf{r}_T|}\frac{e^{-jk|\mathbf{r}-\mathbf{r}_R|}}{|\mathbf{r}-\mathbf{r}_R|}d^3\mathbf{r}. \quad (9)$$

We can perform a four-dimensional Fourier transform with respect to the transmit and receive x and z aperture coordinates, and evaluate this expression asymptotically by the method of stationary phase [20], [34]. The result is a Fourier-domain mapping between the measurement set and target susceptibility:

$$\mathfrak{F}_{4D}\{s\}(k_{xT}, k_{zT}, k_{xR}, k_{zR}) = \frac{-\pi}{k_{yT}k_{yR}}\mathfrak{F}_{3D}\{\chi\}(\mathbf{k}_A) \quad (10)$$

where k_{xT}, k_{zT}, k_{xR}, and k_{zR} are the spatial frequencies defining the Fourier transform of the coherent data set over the transmit and receive coordinates, and each vector $\mathbf{k}_A$ is a point in the three-dimensional k-space representation of χ interrogated by a single transmit/receive antenna pair, with components given by:

$$\begin{aligned} k_{xA} &= k_{xT} + k_{xR} \\ k_{zA} &= k_{zT} + k_{zR} \\ k_{yA} &= k_{yT} + k_{yR} \\ &= \sqrt{k^2 - k_{xT}^2 - k_{zT}^2} + \sqrt{k^2 - k_{xR}^2 - k_{zR}^2}. \end{aligned} \quad (11)$$

Evidently, the target spatial frequencies accessed by the coherent imaging system are simply the sums of the k-values probed by the positions of the transmitter and receiver

pairs that define each measurement. This offers a generalized interpretation of the sum coarray interpretation of a coherent array system. Namely, this result illustrates that the spatial frequency bandpass characteristics of the short-range coherent system consist of a three-dimensional convolution between the transmit and receive aperture spectral decompositions.

Adapting this familiar result from the coherent domain, a similar procedure can be carried out for the passive array system, which obtains visibility measurements described by:

$$v(\mathbf{r}_1, \mathbf{r}_2, k) = \int \varepsilon(\mathbf{r}, k) \frac{e^{jk|\mathbf{r}-\mathbf{r}_1|}}{|\mathbf{r}-\mathbf{r}_1|} \frac{e^{-jk|\mathbf{r}-\mathbf{r}_2|}}{|\mathbf{r}-\mathbf{r}_2|} d^3\mathbf{r}. \quad (12)$$

Here, to remain consistent with the conjugation of the first propagation term, we take an inverse Fourier transform with respect to the first array transverse coordinates x_1 and z_1, followed by a Fourier transform over the second array transverse coordinates x_2 and z_2, which results in a dual mapping between the transformed data set and the Fourier domain of the target spectral density:

$$\mathfrak{F}_{2\mathrm{D}}\left\{\mathfrak{F}_{2\mathrm{D}}^{-1}\{s\}\right\}(k_{x1}, k_{z1}, k_{x2}, k_{z2}) = \frac{-\pi}{k_{y1}k_{y2}} \mathfrak{F}_{3\mathrm{D}}\{\varepsilon\}(\mathbf{k}_P) \quad (13)$$

where k_{x1}, k_{z1}, k_{x2}, k_{z2} are now the spatial frequencies corresponding to the elements in the Fourier transform of the incoherent data set over arrays 1 and 2. The k-space samples interrogated by the incoherent system are now represented by $\mathbf{k}_P$, a three-dimensional vector with components

$$\begin{aligned} k_{xP} &= k_{x1} - k_{x2} \\ k_{zP} &= k_{z1} - k_{z2} \\ k_{yP} &= k_{y1} - k_{y2} \\ &= \sqrt{k^2 - k_{x1}^2 - k_{z1}^2} - \sqrt{k^2 - k_{x2}^2 - k_{z2}^2}. \end{aligned} \quad (14)$$

We see that in the incoherent case, the spatial frequencies probed by the system consist of the difference in the spatial frequencies interrogated by arrays 1 and 2 separately, which generalizes the difference coarray interpretation of the incoherent imaging system. Whereas the coherent bandpass could be constructed by a convolution operation, the k-space structure of the incoherent system is determined by the cross-correlation of the spectral decompositions of arrays 1 and 2, yielding a low-pass behavior consistent with the required Hermitian symmetry of an incoherent transfer function [17], [24], [41], [42].

The distinct k-space structures of these coherent and incoherent imaging systems under a restricted two-dimensional geometry are illustrated in Fig. 3. Here, we assume the aperture exploits all element pairs, so that the achievable spatial frequency components depend only on the operating frequency, aperture extent and aperture sampling. Each point corresponds to the vector sum (Fig. 3(a)) or difference (Fig. 3(b)) of the spatial frequencies probed by a pair of aperture elements. In fact, by employing all aperture pairs, each point can be redundantly described by multiple pair

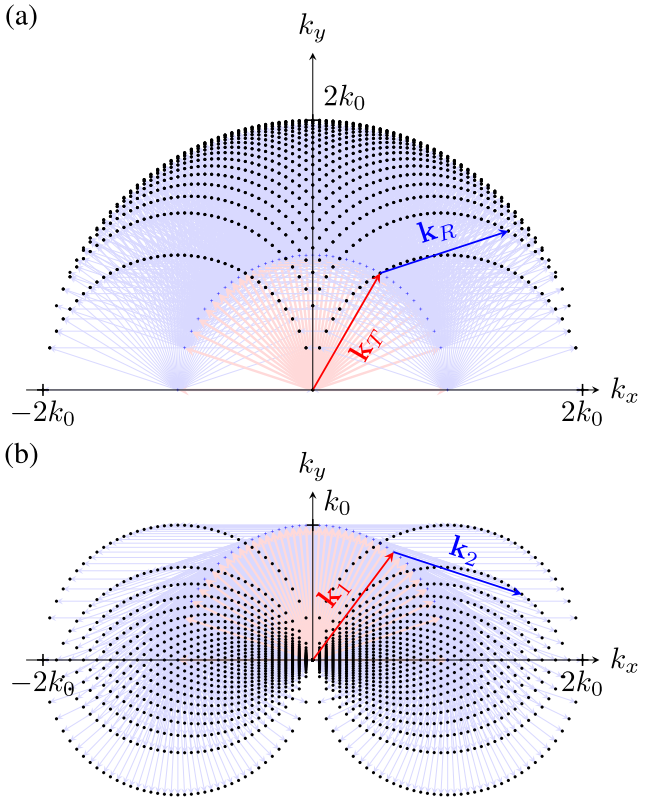

FIGURE 3. Two-dimensional cross sections of the (a) MIMO and (b) SAIR system k-space descriptions, revealing the distinct methods of array synthesis under the two processing approaches.

contributions, an effect that can be alleviated through aperture thinning strategies. As a result of the different k-space synthesis operations, the coherent and incoherent systems cover drastically different regions of the k sphere. Namely, the MIMO support is offset from the origin in the longitudinal (y) direction, whereas the SAIR support is necessarily symmetric about the origin due to the destructive summation of the k vectors.

The k-space structures in Fig. 3 indicate the range of spatial frequencies accessible to diffraction-limited active and passive interferometric systems. A target's signature, meanwhile, occupies a restricted region in either of these domains according to its location and structure. The k-space components constituting the signature of a point target, for example, are determined by the angular extent of the aperture and the relationship between the aperture signal components according to Eq. (11) or (14). For a given aperture, the components of the k vector corresponding to each aperture position can be computed simply by projecting the vector connecting the aperture element to the target position onto the Cartesian axes, as in [43]. That is, the k-space components of target position $\mathbf{r} = (x, y, z)$ interrogated by aperture element n are given by:

$$\begin{aligned} k_{xn} &= k\sin\theta_n\cos\phi_n \\ k_{yn} &= k\cos\theta_n \\ k_{zn} &= k\sin\theta_n\sin\phi_n \end{aligned} \quad (15)$$

where, in our coordinate system orientation, the polar angle θ_n is measured from the positive y axis and the azimuthal angle ϕ_n is measured from the x axis, with the origin taken as the position of array element n. Together, these angles characterize the vector directed from array element n to target position $\mathbf{r}$. In this way, the k-space signature corresponding to a given target location reflects the spatially varying nature of a short-range imaging geometry in addition to the aspect limitations of the finite array.

The formulation outlined in this section offers a simple framework for characterization of short-range image properties. Indeed, many image features can be deduced from the shape, position, and extent of its Fourier transform. The image resolution limit in particular can be defined by a reciprocal relationship to the k-space support:

$$\delta_i = \frac{2\pi}{k_{i,max} - k_{i,min}} \qquad i = x, y, z \tag{16}$$

where δ_i is the half-width resolution in the x, y, or z directions, defined as the distance of the first zero crossing of the sinc function from its peak. Inspection of Fig. 3 reveals that MIMO and SAIR systems have approximately equal resolving capabilities at a given frequency, assuming both systems exploit all array pairs. Evaluation of alternative sparse array configurations is straightforward using the methods proposed in this section, and is carried out in the next section.

In addition to system evaluation and analysis, the method outlined above can be exploited as an efficient Fourier-domain imaging algorithm that generalizes the range migration algorithm, pursued in active systems, to both coherent and incoherent systems. While alternative Fourier-domain methods have been investigated for incoherent systems [37], [44], [45], a direct parallel to the near field range migration algorithm follows from our generalized structure, and has not been proposed, to our knowledge.

Although the general procedure for implementing the Fourier domain algorithm in short-range imaging geometries has been thoroughly described for active MIMO systems in [20], [21], for example, we outline the procedure here for passive SAIR systems, noting that the processing steps are nearly identical. We assume the standard scenario of regularly-sampled two-dimensional arrays, though we note that irregular sampling can be accommodated using non-uniform FFTs [46], [47]. Beginning with the interferometric visibility data represented mathematically by Eq. (8), one computes a four-dimensional FFT over the x and z dimensions of receive arrays 1 and 2, which results in Fourier-domain samples corresponding to spatial frequencies k_{x1}, k_{z1}, k_{x2}, and k_{z2}. The four-dimensional Fourier-domain samples of the visibility data are then mapped to the three spatial frequency components k_{xP}, k_{yP}, and k_{zP} of the target emissivity according to the relationships given in Eq. (14). Following this mapping, the filter term defined by the coefficient on the right-hand side of Eq. (13) is applied, followed by a backpropagation step achieved through multiplication by the term $e^{jk_{yP}y_0}$ with y_0 the approximate distance from the array to the region of interest. At this point, the dataset describes the Fourier transform of the target emissivity over an irregularly sampled set of spatial frequency values. In order to exploit the computational efficiency of the (inverse) FFT, one may interpolate these samples onto a regular grid of spatial frequency values, a step referred to as Stolt interpolation in the active radar literature. This interpolation may be carried out in a variety of ways, but is typically the primary computational bottleneck in $\omega - k$ imaging algorithms [48]. Except where stated, the following results are obtained using a scattered interpolation procedure carried out using the `griddata` function in MATLAB. Once an evenly spaced three-dimensional grid of k values are obtained, the emissivity estimate can be recovered through a three-dimensional inverse FFT. Alternatively, one can recover an image directly from the unevenly sampled data by computing an inverse discrete Fourier transform (DFT). We resort to this latter strategy for the results in Figs. 6 and 8 in order to avoid interpolation artifacts and highlight the distinctions arising from the active versus passive bandpasses.

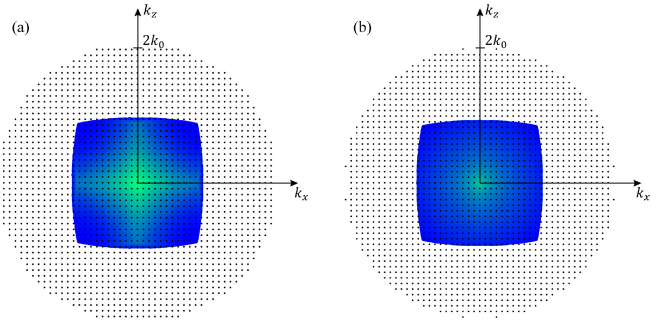

FIGURE 4. Transverse cross sections of aperture and target k-space support for (a) MIMO and (b) SAIR systems at 20 GHz using all antenna pairs in a square aperture with side length 30 cm.

VI. RESULTS

Figures 4 and 5 compare the Fourier-domain signal support and PSF for MIMO and SAIR systems. In Fig. 4, we overlay this signal support for a target position of $\mathbf{r} = (0\text{cm}, 30\text{cm}, 0\text{cm})$ (in blue) onto the total aperture coverage computed for a fully sampled aperture of size 30 cm $\times$ 30 cm operating at 20 GHz and sampled at a quarter wavelength. The k-space structure in the xz plane, depicted in Fig. 4, reveals that MIMO (Fig. 4(a)) and SAIR (Fig. 4(b)) systems probe identical ranges of transverse spatial frequencies. Meanwhile, Fig. 5 illustrates MIMO and SAIR systems coverage for the same array geometry in the xy plane. The insets reveal the full three-dimensional signal structure as a portion of the k-sphere, as well as the corresponding PSF obtained using our proposed imaging algorithm. Figure 5(a) shows the result of performing this procedure for a MIMO array, while Fig. 5(b) gives the response of the corresponding SAIR array. The transverse resolutions in the x and z direction are approximately equal for both the MIMO and SAIR systems as a result

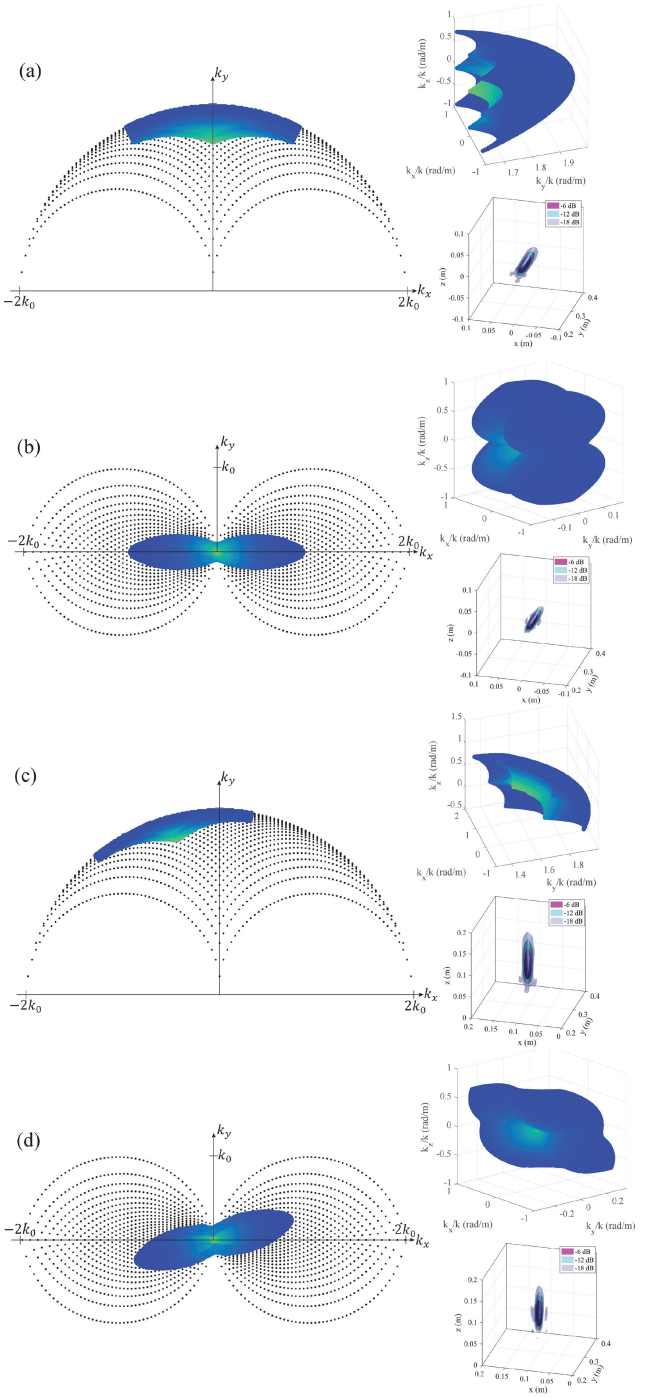

FIGURE 5. Spatially varying *k*-space support in the aperture near field, illustrating an $x - y$ cross section of the signal coverage in the Fourier domain (in blue) overlaid on the total support available to a 30 cm square aperture exploiting all antenna pairs. Inlays reveal the full three-dimensional structure of the Fourier-domain signal and the resulting PSF computed using the proposed algorithm. (a) *k*-space coverage for an active MIMO system at an on-axis point target location of $\mathbf{r} = (0\text{cm}, 30\text{cm}, 0\text{cm})$. (b) *k*-space coverage achieved for the same point target position using a passive SAIR system. (c) Active MIMO system response to an off-axis point target at location $\mathbf{r} = (10\text{cm}, 30\text{cm}, 10\text{cm})$, resulting in shifted and distorted Fourier-domain support and PSF. (d) Similar distortion is evident for the passive SAIR system imaging an off-axis point target. The signal support in the Fourier domain does not shift due to Hermitian symmetry requirements of the incoherent transfer function.

of the square array geometry, while the resolution attained along any dimension is comparable under MIMO or SAIR operation, as predicted by the similar extent of k values

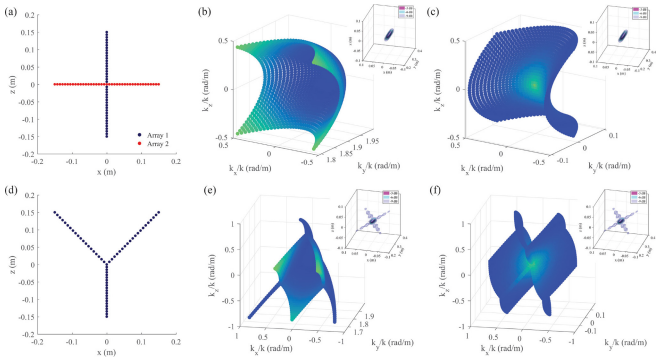

FIGURE 6. (a) Mill's cross geometry utilizing two linear subarrays 1 and 2, resulting in short-range *k*-space coverage illustrated in (b) for a MIMO systems and (c) for a SAIR system. (d) A "Y" array and its generalized short-range coarray for (e) MIMO and (f) SAIR systems.

achieved in Figs. 4 and 5(a) and (b). Both systems suffer from poor longitudinal resolution resulting from the limited view achieved by the arrays along that axis, determined strictly from geometric considerations. This is referred to as the missing cone problem in optical systems [49]. This resolution is typically improved in active systems through coherent synthesis of broadband frequency components [33], [50], whereas incoherent systems must rely on alternative prior information [51].

While the image properties of a far-field imaging system depend only on the transverse geometry of the aperture, a short-range system exhibits substantial dependence on the target position [52], [53]. This effect can be described in terms of the geometrically defined k vectors, and is illustrated in Fig. 5. As the target (here, defined at a single point) moves from an on-axis location of $\mathbf{r} = (0\text{cm}, 30\text{cm}, 0\text{cm})$ to an off-axis location $\mathbf{r} = (10\text{cm}, 30\text{cm}, 10\text{cm})$, the *k*-space map distorts. The equivalent description in the spatial domain shows that the PSF varies accordingly as a result of the limited aperture geometry. Intuitively, the PSF "smears" along the longitudinal direction, an effect remedied by transforming to projective coordinates in [44]. Of course, this spatially variant characteristic implies that the image of an extended target cannot be described by a simple convolution operation [41]. Instead, the image will contain contributions from a potentially large range of distinct PSFs.

The previous results outline general properties of short-range array systems by applying reciprocal space analysis to optimally sampled, dense arrays. Nevertheless, the same approach can be applied to the optimization of sparse arrays through three-dimensional spatial frequency domain synthesis. Figure 6 demonstrates the application of different aperture synthesis techniques in the aperture near field. The Mill's cross aperture geometry employs two perpendicular linear subarrays, and is shown in Fig. 6(a). The coherent system *k*-space map is plotted in Fig. 6(b), and that of the incoherent system in Fig. 6(c). The transverse and longitudinal extents are identical for each, leading to qualitatively similar PSFs as observed in the insets. As mentioned above, these PSFs were computed by directly applying a

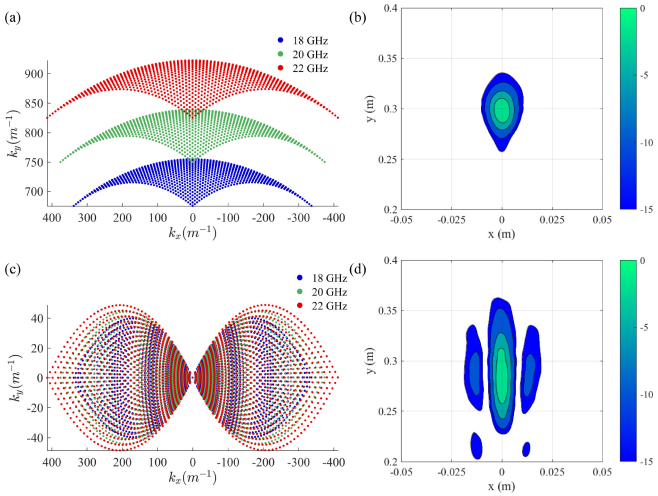

FIGURE 7. ***k*-space coverage and imaging simulation results for a point target at r = (30cm, 0cm, 0cm). (a) MIMO *k*-space coverage at 18 GHz, 20 GHz, and 22 GHz, illustrating the extension of the bandpass along the range direction resulting from coherent synthesis of the broadband signals. (b) Two-dimensional PSF in the range and cross-range dimensions obtained by applying the coherent Fourier-domain reconstruction algorithm to simulated data taken over the 18-22 GHz at 200 MHz spacing. Range resolution is enhanced through the use of a broadband signal, corresponding to the enhanced *k*-space coverage. (c) SAIR *k*-space coverage analogous to the case presented in (a). In this case, incoherent synthesis results in destructive summation of the *k* vectors, leading to poor longitudinal resolution as illustrated in (d).**

DFT to the spatial frequency values illustrated in Fig. 6(b) and (c). In the far field limit, the k-space structures become identical and are referred to respectively as the sum and difference coarrays. Another commonly used sparse array, the Y-array, is illustrated in Fig. 6(d), along with its coherent (Fig. 6(e)) and incoherent (Fig. 6(f)) k-space mappings. These results provide further evidence that the k-space structures comprise short-range generalizations of the sum and difference coarray interpretations for coherent and incoherent systems. Indeed, the transverse profiles agree with the far field coarrays reported in [24].

The bandpass characteristics demonstrated in the previous examples derive strictly from the relationship between the aperture-scene geometry and the wavenumber at a single frequency. The nature of the system leads to distinct k-space representations resulting from either the constructive or destructive synthesis of the spatial frequency vectors. This same process dictates the ability of the two systems to synthesize range information from broadband signals, as illustrated for a 30 cm-long, one-dimensional aperture in Fig. 7. It is conventionally understood that an active, radar system can retrieve range information from broadband or pulsed signals [54]. A near-field MIMO system can evidently obtain range information directly from the system geometry (Fig. 5), though broadband signals will enhance this capability. This can be interpreted through the coherent processing of the range of wavenumbers accessed over the operating frequency, which leads to a series of bandpass structures stacked along the k_y direction, each with radius $2k$ [43]. Figure 7(a) demonstrates that as the bandwidth increases, the k-space coverage along the range direction improves, resulting in improved range resolution in the image. Figure 7(b) shows the reconstructed image of a point target located at $\mathbf{r} = (30\text{cm}, 0\text{cm}, 0\text{cm})$, and interrogated with a broadband signal over the range 18-22 GHz and sampled at 200 MHz intervals. The coherent Fourier-domain algorithm described in Section V was used to reconstruct this target according to the mapping in Eq. (11). The range resolution defined as the half-power beam width in this example is 4.23 cm, and should approximately correspond to the k-space coverage by Eq. (16). Obtaining the maximum and minimum k_y values over the signal bandwidth from Fig. 7(a) gives an expected full-width resolution of 5.08 cm. In contrast to this result, the incoherent system can obtain range information only from the system geometry, and synthesis of broadband information does not augment its Fourier-domain coverage (Fig. 7(c)), as expected for an incoherent system. Therefore the longitudinal signal support is limited to a length of $2k_{max}$ regardless of bandwidth, so that range resolution for a broadband system is determined strictly by its highest operating frequency in the same way as a monochromatic system. The full-width range resolution expected from Fig. 7(c) is thus 12.92 cm, which is comparable to the value 9.35 cm observed in the Fourier-domain reconstruction of Fig. 7(d). Deviations of the observed resolutions from those predicted by Eq. (16) can be attributed to the different definitions used in quantifying resolution. Whereas Eq. (16) defines the expected resolution in terms of zero crossings of the sinc function, our choice of quantifying resolution by full width at half maximum stems from numerical inaccuracies that make such zero crossings difficult to observe, and leads to a systematic underestimate of the image resolution.

The results of applying our generalized Fourier-domain imaging algorithm to an extended target in the array near field are given in Fig. 8. The target consists of three bars of varying orientation 30 cm from the aperture plane. The top row gives the result obtained by the MIMO system in a (a)front and (b)isometric view, and the bottom row shows the SAIR system reconstruction in a (c)front and (d)isometric view. In order to emphasize the role of the mappings defined in Eqs. (10) and (13) independent of the choice of interpolation procedure, these images were computed by DFTs applied to the unevenly spaced samples resulting directly from the relationships of Eqs. (11) and (14). This result highlights the effect of the different processing strategies on overall image characteristics. Namely, the disparate image properties, including an observably stronger background in the incoherent image [55], arise from the particular filtering achieved in the spatial frequency domain according to Eqs. (11) and (14).

VII. DISCUSSION

The reciprocal space framework developed in this paper exploits the analogy between active and passive systems in order to provide an analytical design tool for short-range array systems, generalizing the well-known coarray

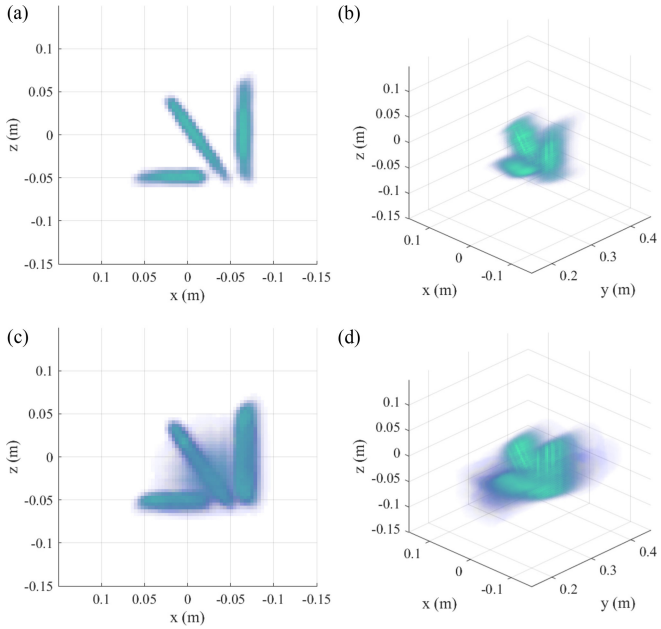

FIGURE 8. Numerically computed three dimensional image reconstructions of three bars at $y = 30$cm using the proposed method. The top row illustrates the reconstruction obtained by a 30 cm × 30 cm MIMO array in a (a) front view, and (b) isometric view. The bottom row depicts the results achieved using a SAIR array of the same size in a (c) front view and (d) isometric view.

methodology. For simplicity, we have not included considerations of the antenna gain/radiation patterns, but have restricted the formalism to arrays consisting of identical, isotropic antennas. This approach highlights the geometric considerations of array design that are the focus of our studies. Nevertheless, the effects of directional radiation patterns can be incorporated into our framework through spatial frequency-domain filter terms, as described in [30].

The results provided in the previous sections explore the effects of the Fourier domain system filters on image resolution and qualitative characteristics. Further investigations may reveal classes of targets that are ideally suited for imaging by either of these modalities independently, in addition to methods by which active and passive system data sets may be coordinated to yield improved hybrid image performance [56].

VIII. CONCLUSION

In this work, we have investigated the shared mathematical structure in the signal models of active MIMO and passive SAIR imaging systems. This has allowed a unified analytical framework for short-range geometries using coarray concepts described in the spatial frequency domain, as well as an efficient Fourier-domain imaging algorithm inspired by strategies employed in active radar systems. We have demonstrated that the short-range, three-dimensional imaging performance of active and passive systems are comparable, though passive systems exhibit poor range resolution compared to active systems that can coherently synthesize frequency data. This methodology can improve predictive modeling techniques for designing short-range imaging architectures and sparse array designs, while simultaneously offering a simple and robust strategy for numerical image reconstruction.

REFERENCES

[1] X. Zhuge, A. G. Yarovoy, T. Savelyev, and L. Ligthart, "Modified kirchhoff migration for UWB MIMO array-based radar imaging," *IEEE Trans. Geosci. Remote Sens.*, vol. 48, no. 6, pp. 2692–2703, Jun. 2010.

[2] J. Gollub *et al.*, "Large metasurface aperture for millimeter wave computational imaging at the human-scale," *Sci. Rep.*, vol. 7, Feb. 2017, Art. no. 42650.

[3] S. S. Ahmed, A. Schiessl, F. Gumbmann, M. Tiebout, S. Methfessel, and L. Schmidt, "Advanced microwave imaging," *IEEE Microw. Mag.*, vol. 13, no. 6, pp. 26–43, Sep./Oct. 2012.

[4] W. F. Moulder *et al.*, "Development of a high-throughput microwave imaging system for concealed weapons detection," in *Proc. IEEE Int. Symp. Phased Array Syst. Technol. (PAST)*, 2016, pp. 1–6.

[5] T. S. Ralston, G. L. Charvat, and J. E. Peabody, "Real-time through-wall imaging using an ultrawideband multiple-input multiple-output (MIMO) phased array radar system," in *Proc. IEEE Int. Symp. Phased Array Syst. Technol.*, 2010, pp. 551–558.

[6] W. Zhang and A. Hoorfar, "Three-dimensional synthetic aperture radar imaging through multilayered walls," *IEEE Trans. Antennas Propag.*, vol. 62, no. 1, pp. 459–462, Jan. 2014.

[7] T. Fromenteze, M. Boyarsky, J. Gollub, T. Sleasman, M. Imani, and D. R. Smith, "Single-frequency near-field MIMO imaging," in *Proc. 11th Eur. Conf. Antennas Propag. (EUCAP)*, 2017, pp. 1415–1418.

[8] C. E. Yarman and B. Yazici, "Synthetic aperture hitchhiker imaging," *IEEE Trans. Image Process.*, vol. 17, pp. 2156–2173, 2008.

[9] N. A. Salmon, "3-D radiometric aperture synthesis imaging," *IEEE Trans. Microw. Theory Techn.*, vol. 63, no. 11, pp. 3579–3587, Nov. 2015.

[10] E. Kpre, C. Decroze, M. Mouhamadou, and T. Fromenteze, "Computational imaging for compressive synthetic aperture interferometric radiometer," *IEEE Trans. Antennas Propag.*, vol. 66, no. 10, pp. 5546–5557, Oct. 2018.

[11] A. V. Diebold, M. F. Imani, T. Fromenteze, D. L. Marks, and D. R. Smith, "Passive microwave spectral imaging with dynamic metasurface apertures," *Optica*, vol. 7, no. 5, pp. 527–536, 2020.

[12] N. A. Salmon, "Indoor full-body security screening: Radiometric microwave imaging phenomenology and polarimetric scene simulation," *IEEE Access*, vol. 8, pp. 144621–144637, 2020.

[13] P. M. Holl and F. Reinhard, "Holography of Wi-Fi radiation," *Phys. Rev. Lett.*, vol. 118, no. 18, 2017, Art. no. 183901.

[14] S. Vakalis, L. Gong, and J. A. Nanzer, "Imaging with WiFi," *IEEE Access*, vol. 7, pp. 28616–28624, 2019.

[15] G. Lockwood and F. S. Foster, "Design of sparse array imaging systems," in *Proc. IEEE Ultrasonics Symp. Int. Symp.*, vol. 2, 1995, pp. 1237–1243.

[16] G. R. Lockwood, P.-C. Li, M. O'Donnell, and F. S. Foster, "Optimizing the radiation pattern of sparse periodic linear arrays," *IEEE Trans. Ultrason., Ferroelect., Freq. Control*, vol. 43, no. 1, pp. 7–14, Jan. 1996.

[17] X. Zhuge and A. G. Yarovoy, "Study on two-dimensional sparse MIMO UWB arrays for high resolution near-field imaging," *IEEE Trans. Antennas Propag.*, vol. 60, no. 9, pp. 4173–4182, Sep. 2012.

[18] S. S. Ahmed, A. Schiess, and L.-P. Schmidt, "Near field mm-Wave imaging with multistatic sparse 2D-arrays," in *Proc. Eur. Radar Conf. (EuRAD)*, 2009, pp. 180–183.

[19] M. Soumekh, *Fourier Array Imaging*. Englewood Cliffs, NJ, USA: Prentice-Hall, 1994.

[20] J. M. Lopez-Sanchez and J. Fortuny-Guasch, "3-D radar imaging using range migration techniques," *IEEE Trans. Antennas Propag.*, vol. 48, no. 5, pp. 728–737, May 2000.

[21] X. Zhuge and A. G. Yarovoy, "Three-dimensional near-field MIMO array imaging using range migration techniques," *IEEE Trans. Image Process.*, vol. 21, pp. 3026–3033, 2012.

[22] A. V. Diebold, L. Pulido-Mancera, T. Sleasman, M. Boyarsky, M. F. Imani, and D. R. Smith, "Generalized range migration algorithm for synthetic aperture radar image reconstruction of metasurface antenna measurements," *J. Opt. Soc. America B*, vol. 34, no. 12, pp. 2610–2623, 2017.

[23] T. Fromenteze, O. Yurduseven, F. Berland, C. Decroze, D. R. Smith, and A. G. Yarovoy, "A transverse spectrum deconvolution technique for MIMO short-range fourier imaging," *IEEE Trans. Geosci. Remote Sens.*, vol. 57, no. 9, pp. 6311–6324, Sep. 2019.
[24] R. T. Hoctor and S. A. Kassam, "The unifying role of the coarray in aperture synthesis for coherent and incoherent imaging," *Proc. IEEE*, vol. 78, no. 4, pp. 735–752, Apr. 1990.
[25] N. Viswanathan, S. Venkatesh, and D. Schurig, "Optimization of a sparse aperture configuration for millimeter-wave computational imaging," *IEEE Trans. Antennas Propag.*, vol. 69, no. 2, pp. 1107–1117, Feb. 2021.
[26] D. Bliss and K. Forsythe, "Multiple-input multiple-output (MIMO) radar and imaging: Degrees of freedom and resolution," in *Proc. 37th Asilomar Conf. Signals Syst. Comput.*, vol. 1, 2003, pp. 54–59.
[27] D. Bliss *et al.*, "GMTI MIMO radar," in *Proc. Int. Waveform Diversity Design Conf.*, 2009, pp. 118–122.
[28] I. Corbella, N. Duffo, M. Vall-Llossera, A. Camps, and F. Torres, "The visibility function in interferometric aperture synthesis radiometry," *IEEE Trans. Geosci. Remote Sens.*, vol. 42, no. 8, pp. 1677–1682, Aug. 2004.
[29] C. Cafforio, C. Prati, and F. Rocca, "SAR data focusing using seismic migration techniques," *IEEE Trans. Aerosp. Electron. Syst.*, vol. 27, no. 2, pp. 194–207, Mar. 1991.
[30] M. Soumekh, "Echo imaging using physical and synthesized arrays," *Opt. Eng.*, vol. 29, no. 5, pp. 545–555, 1990.
[31] D. M. Sheen, D. L. McMakin, W. M. Lechelt, and J. W. Griffin, "Circularly polarized millimeter-wave imaging for personnel screening," in *Proc. Passive Millimeter-Wave Imag. Technol. VIII*, vol. 5789, 2005, pp. 117–126.
[32] J. Laviada, A. Arboleya-Arboleya, Y. Álvarez, B. González-Valdés, and F. Las-Heras, "Multiview three-dimensional reconstruction by millimetre-wave portable camera," *Sci. Rep.*, vol. 7, no. 1, pp. 1–11, 2017.
[33] D. M. Sheen, D. L. McMakin, and T. E. Hall, "Three-dimensional millimeter-wave imaging for concealed weapon detection," *IEEE Trans. Microw. Theory Techn.*, vol. 49, no. 9, pp. 1581–1592, Sep. 2001.
[34] W. C. Chew, *Waves and Fields in Inhomogeneous Media*. New York, NY, USA: IEEE Press, 1995.
[35] R. E. Collin, *Field Theory of Guided Waves*, vol. 5. New York, NY, USA: Wiley, 1990.
[36] D. L. Marks, J. Gollub, and D. R. Smith, "Spatially resolving antenna arrays using frequency diversity," *J. Opt. Soc. America A*, vol. 33, no. 5, pp. 899–912, 2016.
[37] J. Chen, Y. Li, J. Wang, Y. Li, and Y. Zhang, "An accurate imaging algorithm for millimeter wave synthetic aperture imaging radiometer in near-field," *Progr. Electromagn. Res.*, vol. 141, pp. 517–535, Jan. 2013.
[38] J. W. Goodman, *Statistical Optics*. New York, NY, USA: Wiley, 2015.
[39] L. Mandel and E. Wolf, *Optical Coherence and Quantum Optics*. Cambridge, U.K.: Cambridge Univ. Press, 1995.
[40] A. R. Thompson, J. M. Moran, and G. W. Swenson, *Interferometry and Synthesis in Radio Astronomy*. New York, NY, USA: Wiley, 1986.
[41] J. W. Goodman, *Introduction to Fourier Optics*. Greenwood Village, CO, USA: Roberts Company Publ., 2005.
[42] A. V. Diebold, M. F. Imani, T. Sleasman, and D. R. Smith, "Phaseless coherent and incoherent microwave ghost imaging with dynamic metasurface apertures," *Optica*, vol. 5, no. 12, pp. 1529–1541, 2018.
[43] S. S. Ahmed, *Electronic Microwave Imaging with Planar Multistatic Arrays*. Berlin, Germany: Logos Verlag GmbH, 2014.
[44] D. L. Marks, R. A. Stack, and D. J. Brady, "Three-dimensional coherence imaging in the Fresnel domain," *Appl. Opt.*, vol. 38, no. 8, pp. 1332–1342, 1999.
[45] W. Carter, "On refocusing a radio telescope to image sources in the near field of the antenna array," *IEEE Trans. Antennas Propag.*, vol. 37, no. 3, pp. 314–319, Mar. 1989.
[46] Q. H. Liu and N. Nguyen, "An accurate algorithm for nonuniform fast Fourier transforms (NUFFT's)," *IEEE Microw. Guided Wave Lett.*, vol. 8, no. 1, pp. 18–20, Jan. 1998.
[47] J. Song, Q. H. Liu, P. Torrione, and L. Collins, "Two-dimensional and three-dimensional NUFFT migration method for landmine detection using ground-penetrating radar," *IEEE Trans. Geosci. Remote Sens.*, vol. 44, no. 6, pp. 1462–1469, Jun. 2006.
[48] I. Cumming, F. Wong, and K. Raney, "A sar processing algorithm with no interpolation," in *Proc. Int. Geosci. Remote Sens. Symp.*, vol. 1, 1992, pp. 376–379.
[49] D. A. Agard, Y. Hiraoka, P. Shaw, and J. W. Sedat, "Fluorescence microscopy in three dimensions," in *Methods in Cell Biology*, vol. 30. New York, NY, USA: Elsevier, 1989, pp. 353–377.
[50] M. Soumekh, *Synthetic Aperture Radar Signal Processing*, vol. 7. New York, NY, USA: Wiley, 1999.
[51] J. Lim *et al.*, "Comparative study of iterative reconstruction algorithms for missing cone problems in optical diffraction tomography," *Opt. Exp.*, vol. 23, no. 13, pp. 16933–16948, 2015.
[52] M. Soumekh, "Depth-focused interior echo imaging," *IEEE Trans. Image Process.*, vol. 8, pp. 1608–1618, 1999.
[53] M. A. Maisto, R. Pierri, and R. Solimene, "Near-field transverse resolution in planar source reconstructions," *IEEE Trans. Antennas Propag.*, vol. 69, no. 8, pp. 4836–4845, Aug. 2021.
[54] M. I. Skolnik, *Introduction to Radar Systems*, vol. 3. New York, NY, USA: McGraw-Hill, 1980.
[55] A. V. Diebold, J. B. Pendry, A. Favaro, M. F. Imani, and D. R. Smith, "Spatial coherence in 2D holography," *J. Opt. Soc. America A*, vol. 38, no. 5, pp. 727–736, 2021.
[56] M. Piles, D. Entekhabi, and A. Camps, "A change detection algorithm for retrieving high-resolution soil moisture from smap radar and radiometer observations," *IEEE Trans. Geosci. Remote Sens.*, vol. 47, no. 12, pp. 4125–4131, Dec. 2009.

AARON V. DIEBOLD received the B.S. degree in physics and mathematics and the M.S. degree in electrical engineering from the University of Cincinnati, Cincinnati, OH, USA, in 2014 and 2016, respectively, and the Ph.D. degree from the Department of Electrical and Computer Engineering, Duke University, Durham, NC, USA, in 2020.

He is currently a Postdoctoral Associate with the Center for Metamaterials and Integrated Plasmonics, Duke University. His current research interests include active and passive imaging, holography, and metasurface design.

THOMAS FROMENTEZE received the Ph.D. degree from the University of Limoges, Limoges, France, in 2015.

From 2015 to 2016, he was a Postdoctoral Researcher with Duke University, Durham, NC, USA. He is currently a Maître de Conférences (an Associate Professor) with the XLIM Research Institute, University of Limoges. He is also an Adjunct Assistant Professor with the Center for Metamaterials and Integrated Plasmonics, Duke University. His research interests include ultra-wideband microwave and millimeter-wave imaging, wave propagation in complex media, computational/compressive imaging, and the various associated inverse problems.

Dr. Fromenteze received the 11th EuRAD Young Engineer Prize during the European Microwave Week 2015.

ETTIEN KPRÉ received the M.S. and Ph.D. degrees in electronics and electrical engineering from the University of Limoges, Limoges, France, in 2014 and 2017, respectively.

He is currently a Research Engineer with the MC2-Technologies of Lille, Sainghin-en-Mélantois, France. His current research interests include active and passive millimeter-wave imaging, compressive sensing and the associated inverse problems, and multiple input multiple output and FMCW radar signal processing.

Dr. Kpré received the IEEE Ulrich Rhodes Best Innovative Paper during the 2016 IEEE International Conference on Antenna Measurements and Applications, Syracuse, NY, USA.

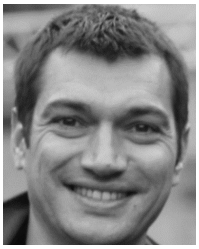

CYRIL DECROZE received the Ph.D. degree in telecommunications engineering from the University of Limoges, France, in 2002.

He is currently a Professor with the XLIM Research Institute, where he has been the Head of the Antennas and Signal Team since 2016. From 2015 to 2019, he was the Coordinator of the PIXEL Project on millimeter waves interferometric imaging systems, and funded by the French National Research Agency. He has been involved in more than 25 research projects at the national and European levels, and has co-supervised 15 Ph.D. theses. He has coauthored four patents, and more than 100 peer-reviewed journal articles and conference papers. His field of research concerns multiple antennas systems, and associated processing for communications and radar imaging.

MOHAMMADREZA F. IMANI (Member, IEEE) received the B.S.E. degree in electrical engineering from the Sharif University of Technology, Tehran, Iran, in 2007, and the M.S.E. and Ph.D. degrees in electrical engineering from the University of Michigan, Ann Arbor, MI, USA, in 2010 and 2013, respectively. From 2014 to 2018, he has served as a Postdoctoral Associate and a Research Scientist with the Department of Electrical and Computer Engineering, Duke University, Durham, NC, USA. He is currently an Assistant Professor with the School of Electrical, Computer, and Energy Engineering, Arizona State University, Tempe, AZ, USA. His research interests include analytical and applied electromagnetics, metamaterials and metasurfaces, microwave imaging and sensing, and MIMO communication systems.

DAVID R. SMITH (Senior Member, IEEE) is the James B. Duke Distinguished Professor of the Electrical and Computer Engineering Department, Duke University, where he also serves as the Director of the Center for Metamaterial and Integrated Plasmonics. He has provided extensive contributions to the field of metamaterials, his team having fabricated and characterized the first "Negative Index" metamaterial in 2000. This experiment introduced the term "Metamaterial" in the context of designed electromagnetic circuits, as well as the concept of negative refraction. In 2006, he has coauthored a paper describing the technique of "Transformation Optics"—a design tool that could leverage the unique properties of metamaterials. As a compelling example of the potential of transformation optics to achieve novel devices, a metamaterial "Invisibility Cloak" was proposed and later demonstrated by his lab that same year. His interests in solving real-world problems have led to the demonstrations of full metamaterial-based systems, with innovations in security scanning; satellite-based synthetic aperture radar; human presence detection; wireless power transfer; wireless communications; through-wall imaging; and many others. As part of this effort, he has a Co-Founded or helped launch numerous metamaterial-based startups, including MetacCept Corp., of which he is CEO. His research interests include the theory, simulation and characterization of structured materials across the electromagnetic spectrum, including photonic crystals, metamaterials and plasmonic nanostructures, as well as applications that leverage these unique materials. He has been recognized for his contributions to metamaterials, first a co-recipient of the Descartes Research Prize in 2005, awarded by the European Union, and later a co-recipient of the McGroddy Prize for New Materials, awarded by the American Physical Society, for "The Discovery of Metamaterials" (2013). In 2016, he was elected to the National Academy of Inventors. In 2021, he has been shortlisted for the A. F. Harvey Engineering Research Prize, awarded by the IET. In 2009, he was named a "Citation Laureate" by Clarivate Web of Knowledge, for having among the most number of Highly Cited papers in the field of Physics over the past decade; he has remained on the list ever since. He has also taken a role in transitioning metamaterial concepts into viable engineering technologies, having contributed to the largescale commercialization of metamaterial devices and components.